Hydrol. Earth Syst. Sci. Discuss., 10, 9191–9238, 2013
www.hydrol-earth-syst-sci-discuss.net/10/9191/2013/
doi:10.5194/hessd-10-9191-2013

Hydrology and Earth System Sciences
Discussions
Open Access

Linking the river to the estuary: influence of river discharge on tidal damping

H. Cai[1], **H. H. G. Savenije**[1], **and M. Toffolon**[2]

[1]Department of Water Management, Faculty of Civil Engineering and Geosciences, Delft University of Technology, Stevinweg 1, P.O. Box 5048, 2600 GA Delft, the Netherlands
[2]Department of Civil, Environmental and Mechanical Engineering, University of Trento, Trento, Italy

Received: 26 June 2013 – Accepted: 8 July 2013 – Published: 15 July 2013

Correspondence to: H. Cai (h.cai@tudelft.nl)

Published by Copernicus Publications on behalf of the European Geosciences Union.

Abstract

The effect of river discharge on tidal damping in estuaries is explored within one consistent theoretical framework where analytical solutions are obtained by solving four implicit equations, i.e., the phase lag, the scaling, the damping and the celerity equation. In this approach the damping equation is obtained by subtracting the envelope curves of high water and low water occurrence, taking into account that the flow velocity consists of a tidal and river discharge component. Different approximations of the friction term are considered in deriving the damping equation, resulting in as many analytical solutions. In this framework it is possible to show that river discharge affects tidal damping primarily through the friction term. The application to the Modaomen and Yangtze estuaries demonstrates that the influence of river discharge on tidal damping can be significant in the upstream part of an estuary where the ratio of river flow to tidal flow amplitude is substantial. The analytical model is able to describe the main tidal dynamics with realistic roughness values in the upper part of the estuary, while a model with negligible river discharge can be made to fit observations only with unrealistically high roughness values. Moreover, the damping equation can be used to estimate river discharge on the basis of observed tidal damping, which makes the proposed analytical model a tool to obtain indirect information about quantities that are difficult to measure in the tidal region.

1 Introduction

The natural variability of river flow into estuaries is greatly modified by human activities, such as dam construction, flow diversion and freshwater withdrawal. These activities impact on tidal damping and tidal wave propagation. In addition, they influence salt intrusion and even storm surge propagation into an estuary (Zhang et al., 2011, 2012; Cai et al., 2012b). Hence, understanding the effect of river discharge on tidal hydraulics is important. Most studies on the analytical solution of tidal wave propaga-

HESSD
10, 9191–9238, 2013

tion neglect the effect of river discharge, such as Hunt (1964), Dronkers (1964), Ippen (1966), Friedrichs and Aubrey (1994), Savenije (1998, 2001), Lanzoni and Seminara (1998), Prandle (2003), Savenije et al. (2008), Toffolon and Savenije (2011), Van Rijn (2011) and Cai et al. (2012a). Only few studies analysed the influence of river discharge on tidal wave propagation in estuaries. Of these, most authors used perturbation analysis, where the scaled equations are simplified by neglecting higher order terms, generally discarding the advective acceleration term and linearizing the friction term (e.g., Dronkers, 1964; Leblond, 1978; Godin, 1985, 1999; Jay, 1991). Others used a regression model to determine the relationship between river discharge and tide (Jay et al., 2011; Kukulka and Jay, 2003). In contrast, Horrevoets et al. (2004) and Cai et al. (2012b) provided analytical solutions of tidal damping accounting for the effect of river discharge without simplifying the equations, based on the envelope method originally developed by Savenije (1998).

The treatment of the nonlinear friction term is key to finding an analytical solution for tidal hydrodynamics. The nonlinearity of the friction term has two sources: the quadratic stream velocity in the numerator and the variable hydraulic radius in the denominator (Parker, 1991). The classical linearization of the friction term was first obtained by Lorentz (1926) who, disregarding the variable depth, equated the dissipation by the linear friction over the tidal cycle to that of the quadratic friction. An extension to include river discharge was provided by Dronkers (1964). In this seminal work, he derived a higher order formulation using Chebyshev polynomials, both with and without river discharge, resulting in a close correspondence with the quadratic velocity. Godin (1991, 1999) showed that quadratic velocity can be well approximated by using only the first and third order terms of the non-dimensional velocity. However, none of the above linearizations took into account the effect of the periodic variation of the hydraulic radius (to the power 4/3 in the Manning–Strickler formulation) in the denominator of the friction term. On the other hand, Savenije (1998), using the envelope method (see Appendix A), obtained a damping equation that takes account of both the quadratic velocity and the time-variable hydraulic radius in the denominator.

HESSD
10, 9191–9238, 2013

Recently, Cai et al. (2012a) proposed a framework for the analysis of tidal wave propagation that allows for different friction formulations. However, the effect of river discharge was not yet included. Here we extend the framework to account for river discharge using different approximations of the friction term. Substituting these approximations in the damping equation, by means of the envelope method, results in an equal number of analytical solutions, which can be readily combined within the analytical framework of Cai et al. (2012a).

In the following section, we introduce the relevant dimensionless parameters that control tidal hydrodynamics. The analytical framework for tidal wave propagation is summarized in Sect. 3. The damping equations that take account of river discharge are presented in Sect. 4. Section 5 presents a comparison of the different analytical approaches and a sensitivity analysis. The model is subsequently applied to two real estuaries where the effect of the river discharge is apparent in the upstream part of the estuary. In addition, we propose a new method to estimate river discharge for observed tidal damping. The paper closes off with conclusions in Sect. 6.

2 Formulation of the problem

We consider a tidal channel with varying width and depth, a mostly rectangular cross section and lateral storage areas described by the storage width ratio $r_S = B_S/\overline{B}$, which is the ratio between the storage width B_S and the average stream width $\overline{B}$ (hereafter overbars denote tidal averages). The geometry of the idealized tidal channel is described in Fig. 1, together with a simplified picture of the periodic oscillations of water level and velocity defining the phase lag. It is generally accepted that the main geometric parameters of alluvial estuaries (tidally averaged cross-sectional area, width and depth) can be well described by exponential functions (e.g., Savenije, 1992):

$$\overline{A} = \overline{A_0}\exp\left(-\frac{x}{a}\right), \qquad \overline{B} = \overline{B_0}\exp\left(-\frac{x}{b}\right), \qquad \overline{h} = \overline{h_0}\exp\left(-\frac{x}{d}\right), \tag{1}$$

HESSD
10, 9191–9238, 2013

where x is the longitudinal coordinate directed landward, $\overline{A}$ and $\overline{h}$ are the tidally averaged cross-sectional area and flow depth, a, b, d are the convergence length of the cross-sectional area, width, and depth, respectively, and the subscript 0 relates to the reference point near the estuary mouth. It follows from $\overline{A} = \overline{B}\,\overline{h}$ that $a = bd/(b+d)$.

The one-dimensional hydrodynamic equations in an alluvial estuary are given by (e.g., Savenije, 2005, 2012):

$$\frac{\partial U}{\partial t} + U\frac{\partial U}{\partial x} + g\frac{\partial h}{\partial x} + gI_b + gF + \frac{gh}{2\rho}\frac{\partial \rho}{\partial x} = 0, \tag{2}$$

$$r_s\frac{\partial h}{\partial t} + U\frac{\partial h}{\partial x} + h\frac{\partial U}{\partial x} + \frac{hU}{\overline{B}}\frac{\partial \overline{B}}{\partial x} = 0, \tag{3}$$

where t is the time, U is the cross-sectional average flow velocity, h is the flow depth, g is the gravitational acceleration, I_b is the bottom slope, ρ is the water density and F is the friction term, defined as:

$$F = \frac{U|U|}{K^2 h^{4/3}}, \tag{4}$$

where K is the Manning–Strickler friction coefficient.

If we define the water level variation $z = h - \overline{h}$, then for a small tidal amplitude to depth ratio, we find:

$$U\frac{\partial h}{\partial x} = U\frac{\partial\left(z+\overline{h}\right)}{\partial x} = U\frac{\partial z}{\partial x} + \frac{\overline{h}U}{\overline{h}}\frac{\partial \overline{h}}{\partial x} \approx U\frac{\partial z}{\partial x} + \frac{hU}{\overline{h}}\frac{\partial \overline{h}}{\partial x}. \tag{5}$$

Substituting Eq. (5) into Eq. (3) and making use of Eq. (1), the following equation is obtained:

$$r_S\frac{\partial z}{\partial t} + U\frac{\partial z}{\partial x} + h\frac{\partial U}{\partial x} - \frac{hU}{a} = 0, \tag{6}$$

HESSD
10, 9191–9238, 2013

which has the advantage that the depth convergence is implicitly taken into account by the convergence of the tidally averaged cross-sectional area.

The system is forced by a harmonic tidal wave with a tidal period T and a frequency $\omega = 2\pi/T$ at the mouth of the estuary. As schematically shown in Fig. 1, the amplitudes of the tidal water level z and velocity U are represented by the variables of η and υ, respectively. The phases of the water level and velocity oscillations are indicated by ϕ_z and ϕ_U, respectively. In a Lagrangean approach, we assume that the water particle moves according to a simple harmonic wave and the influence of river discharge on tidal velocities is not negligible. As a result, the instantaneous flow velocity V for a moving particle is made up of a steady component U_r, created by the discharge of freshwater, and a time-dependent component U_t, contributed by the tide:

$$V = U_t - U_r\,, \qquad U_t = \upsilon \sin(\omega t)\,, \qquad U_r = Q_\mathrm{f}/\overline{A}\,, \tag{7}$$

where Q_f is the freshwater discharge, directed against the positive x-direction.

It can be shown that the estuarine hydrodynamics is controlled by three dimensionless parameters in the case of negligible river discharge (Toffolon et al., 2006; Savenije et al., 2008; Toffolon and Savenije, 2011; Cai et al., 2012a). Table 1 presents these independent dimensionless parameters that depend on the geometry and external forcing. They are: ζ_0 the dimensionless tidal amplitude at the downstream boundary, γ the estuary shape number (representing the effect of cross-sectional area convergence and depth) and χ_0 the reference friction number (describing the frictional dissipation). These parameters contain c_0 representing the classical wave celerity of a frictionless progressive wave in a constant-width channel:

$$c_0 = \sqrt{g\overline{h}/r_\mathrm{S}}\,. \tag{8}$$

The six dependent dimensionless variables are also presented in Table 1. They are: δ the damping number (a dimensionless description of the rate of increase, $\delta > 0$, or decrease, $\delta < 0$, of the tidal wave amplitude along the estuary), μ the velocity number

HESSD
10, 9191–9238, 2013

(the actual velocity scaled with the frictionless value in a prismatic channel), λ the celerity number (the ratio between the theoretical frictionless celerity in a prismatic channel and the actual wave celerity), ε the phase lag between high water (HW) and high water slack (HWS) or between low water (LW) and low water slack (LWS), ζ the dimensionless tidal amplitude that varies along the estuary, and finally χ the friction number as a function of ζ (Toffolon et al., 2006; Savenije et al., 2008). The friction number contains f as the dimensionless friction factor resulting from the envelope method (Savenije, 1998):

$$f = \frac{g}{K^2 \bar{h}^{-1/3}} \left[1 - \left(4\zeta/3\right)^2\right]^{-1}, \tag{9}$$

where the factor 4/3 stems from a Taylor approximation of the exponent of the hydraulic radius in the friction term.

3 Analytical framework for tidal wave propagation with no river discharge

For negligible river discharge, the analytical solution of the one-dimensional hydrodynamic equations is obtained by solving four implicit equations, i.e., the phase lag, the scaling, the celerity and the damping equation (Savenije et al., 2008). The phase lag and scaling equations were derived from the mass balance equation by Savenije (1992, 1993) using a Lagrangean approach. The celerity equation was developed by Savenije and Veling (2005) using a method of characteristics. The damping equation can be obtained through various methods. Savenije (1998, 2001) introduced the envelope method that retains the nonlinear friction term, by subtracting the envelopes at HW and LW.

Cai et al. (2012a) showed that different friction formulations can be used in the envelope method to arrive at an equal number of damping equations. In general, the main classes of the solutions are: (1) quasi-nonlinear solution with nonlinear friction term

HESSD
10, 9191–9238, 2013

(Savenije et al., 2008); (2) linear solution with Lorentz's linearization (Lorentz, 1926); (3) Dronkers' solution with higher order formulation for quadratic velocity (Dronkers, 1964); (4) hybrid solution characterized by a weighted average of Lorentz's linearization, with weight 1/3, and the nonlinear friction term, with weight 2/3 (Cai et al., 2012a). In Table 2, we present the solutions of these four classes for the general case and for some particular cases, including: constant cross-section ($\gamma = 0$), frictionless channel ($\chi = 0$, both with subcritical convergence ($\gamma < 2$) and supercritical convergence ($\gamma \geq 2$)) and ideal estuary ($\delta = 0$). It was shown by Cai et al. (2012a) that the hybrid model provides the best predictions when compared with numerical solutions. Figure 2 shows the main dependent dimensionless parameters as function of the shape number γ and the friction number χ, obtained with the hybrid model.

4 New damping equations accounting for the effect of river discharge

In the following, we extend the validity of the damping equations by introducing the effect of river discharge into the different approximations of the friction term. The dimensionless river discharge φ is defined as:

$$\varphi = \frac{U_r}{U}. \tag{10}$$

We show the procedure for including the effect of river discharge within the envelope method in Appendix A.

For a more concise notation, we refer to a general formulation of the damping parameter of the form:

$$\delta = \frac{\mu^2}{1+\mu^2\beta}\left(\gamma\theta - \chi\mu\lambda\Gamma\right), \tag{11}$$

where we introduce the dimensionless parameters β, θ, and Γ. Both β and θ are equal to unity if $\varphi = 0$. The parameter β corrects the tidal Froude number $\mu^2 = [U/(c_0 r_S \zeta)]^2$

HESSD
10, 9191–9238, 2013

(Savenije et al., 2008) for the influence of river discharge:

$$\beta = \theta - r_S \zeta \frac{\varphi}{\mu\lambda}. \tag{12}$$

The correction factor θ accounts for the wave celerity not being equal at HW and LW, which depends on φ by:

$$\theta = 1 - \left(\sqrt{1+\zeta} - 1\right) \frac{\varphi}{\mu\lambda}. \tag{13}$$

This parameter has a value smaller than unity, but is close to unity as long as $\zeta \ll 1$ although $\mu\lambda = \sin(\varepsilon)$ is also less than 1. In practical applications, we can typically assume $\theta \approx 1$, but this is not a necessary assumption in our method. Finally, the parameter Γ depends on the specific approach, as it is discussed in the next sections.

4.1 The quasi-nonlinear approach

Savenije et al. (2008) presented a fully analytical solution for tidal wave propagation without linearizing the friction term through the envelope method. The method was termed quasi-nonlinear because it still made use of a regular harmonic function to describe the flow velocity. Horrevoets et al. (2004) introduced the effect of river discharge in the quasi-nonlinear model. Using the dimensionless parameters presented in Table 1, Cai et al. (2012b) developed this solution into a general expression for tidal damping, where two zones are distinguished depending on the value of φ defined by Eq. (10).

In the tide-dominated zone, where $\varphi < \mu\lambda$, the parameter Γ introduced in Eq. (11) reads

$$\Gamma = \mu\lambda \left[1 + \frac{8}{3}\zeta \frac{\varphi}{\mu\lambda} + \left(\frac{\varphi}{\mu\lambda}\right)^2\right], \tag{14}$$

HESSD
10, 9191–9238, 2013

while in the river discharge-dominated zone, where $\varphi \geq \mu\lambda$, it becomes

$$\Gamma = \mu\lambda \left[\frac{4}{3}\zeta + 2\frac{\varphi}{\mu\lambda} + \frac{4}{3}\zeta \left(\frac{\varphi}{\mu\lambda} \right)^2 \right] . \quad (15)$$

4.2 Lorentz's approach

The Fourier expansion of the product $U|U|$ in the friction term is (Dronkers, 1964, 272–275):

$$U|U| = \frac{1}{4}L_0 \upsilon^2 + \frac{1}{2}L_1 \upsilon U_t , \quad (16)$$

where the expressions of coefficients L_0 and L_1 when $0 < \varphi < 1$ are:

$$L_0 = [2 + \cos(2\alpha)] \left(2 - \frac{4\alpha}{\pi} \right) + \frac{6}{\pi} \sin(2\alpha) , \quad (17)$$

$$L_1 = \frac{6}{\pi} \sin(\alpha) + \frac{2}{3\pi} \sin(3\alpha) + \left(4 - \frac{8\alpha}{\pi} \right) \cos(\alpha) , \quad (18)$$

with

$$\alpha = \arccos(-\varphi) , \quad (19)$$

where $\pi/2 < \alpha < \pi$ because φ is positive. In case $\varphi \geq 1$,

$$L_0 = -2 - 4\varphi^2, \quad L_1 = 4\varphi , \quad (20)$$

while the case of φ=1 (i.e., $U_r = \upsilon$) corresponds with $\alpha = \pi$ and leads to $L_0 = -6$ and $L_1 = 4$. The Lorentz's coefficients as a function of φ are given in Fig. 3a. The performance of the Lorentz's approximation Eq. (16) to $U|U|$ is shown in Fig. 4.

HESSD
10, 9191–9238, 2013

As a result, the development of the Lorentz's friction term accounting for the effect of river discharge reads:

$$F_{\mathrm{L}} = \frac{1}{K^2 \overline{h}^{4/3}} \left(\frac{1}{4} L_0 \upsilon^2 + \frac{1}{2} L_1 \upsilon U_t \right), \tag{21}$$

where the subscript L stands for Lorentz.

If the river discharge is negligible, i.e., $U_r = 0$ and $\alpha = \pi/2$, Eq. (21) reduces to the classical Lorentz linearization and hence $L_0 = 0$ and $L_1 = 16/(3\pi)$:

$$F_{\mathrm{L}} = \frac{8}{3\pi} \frac{\upsilon}{K^2 \overline{h}^{4/3}} U_t \,. \tag{22}$$

With the envelope method, making use of friction term Eq. (21), it is possible to derive the parameter Γ in the damping Eq. (11) (see Appendix A):

$$\Gamma_{\mathrm{L}} = \frac{L_1}{2} \,. \tag{23}$$

Extending Lorentz's solution with the periodic variation of the depth in the denominator of the friction term (i.e., $K^2 h^{4/3}$) is also possible. The resulting expression is reported in Table 3, where $\kappa = 1$ yields the time-dependent case, while Eq. (20) is recovered by setting $\kappa = 0$.

4.3 Dronkers' approach

The Chebyshev polynomials approach of Dronkers (1964) also provides a way to account for river discharge. It leads to a friction term expressed as:

$$F_{\mathrm{D}} = \frac{1}{K^2 \overline{h}^{4/3} \pi} \left(p_0 \upsilon^2 + p_1 \upsilon U + p_2 U^2 + p_3 U^3 / \upsilon \right), \tag{24}$$

HESSD
10, 9191–9238, 2013

where p_i ($i = 0, 1, 2, 3$) are the Chebyschev coefficients, which depend on φ through α in Eq. (19). They can be expressed as (Dronkers, 1964, p. 301):

$$p_0 = -\frac{7}{120}\sin(2\alpha) + \frac{1}{24}\sin(6\alpha) - \frac{1}{60}\sin(8\alpha),$$
$$p_1 = \frac{7}{6}\sin(\alpha) - \frac{7}{30}(3\alpha) - \frac{7}{30}\sin(5\alpha) + \frac{1}{10}\sin(7\alpha),$$
$$p_2 = \pi - 2\alpha + \frac{1}{3}\sin(2\alpha) + \frac{19}{30}\sin(4\alpha) - \frac{1}{5}\sin(6\alpha),$$
$$p_3 = \frac{4}{3}\sin(\alpha) - \frac{2}{3}\sin(3\alpha) + \frac{2}{15}\sin(5\alpha). \quad (25)$$

The coefficients p_1, p_2 and p_3 determine the magnitude of linear, quadratic and cubic frictional interaction, respectively. Figure 3b shows the Chebyshev coefficients p_0, p_1, p_2 and p_3 as a function of φ. It appears that the values of p_0 are small with respect to the values of the other coefficients; thus this term can usually be neglected. The coefficients p_1 and p_3 decrease with increasing φ until they converge to 0 for $\varphi > 1$. For $\varphi \geq 1$, $p_0 = p_1 = p_3 = 0$ and $p_2 = -\pi$, so that the friction term becomes $F_D = U^2/(K^2 h^{-4/3})$. If $\varphi = 0$, $p_0 = p_2 = 0$, $p_1 = 16/15$ and $p_3 = 32/15$, so that Eq. (24) reduces to

$$F_D = \frac{16}{15\pi}\frac{\upsilon^2}{K^2 h^{-4/3}}\left[\frac{U}{\upsilon} + 2\left(\frac{U}{\upsilon}\right)^3\right], \quad (26)$$

where in this case the subscript D stands for Dronkers. Using Dronkers' friction term Eq. (24) in the envelope method described in Appendix A, we are able to derive the following expression:

$$\Gamma_D = \frac{1}{\pi}\left[p_1 - 2p_2\varphi + p_3\varphi^2\left(3 + \left(\frac{\mu\lambda}{\varphi}\right)^2\right)\right]. \quad (27)$$

HESSD
10, 9191–9238, 2013

Also in this case, the periodic variation of the depth in the friction term can be accounted for by setting $\kappa=1$ in the expression provided in Table 3.

4.4 Godin's approach

For tidal river applications (e.g., the upper Saint Lawrence river), Godin (1991, 1999) showed that an accurate approximation of the friction term can be obtained by using only the first and third order terms of the dimensionless velocity. Adopting this approximation yields:

$$F_{\mathrm{G}} = \frac{16}{15\pi}\frac{U'^2}{K^2\overline{h}^{4/3}}\left[\frac{U}{U'} + 2\left(\frac{U}{U'}\right)^3\right], \tag{28}$$

where subscript G stands for Godin, and U' is defined as

$$U' = \upsilon + U_r\,. \tag{29}$$

Equation (28) is very similar to Eq. (26), the difference being that in Dronkers' approach U is made dimensionless by the tidal velocity amplitude υ, while Godin does this with the maximum possible velocity U'. We can see in Fig. 4 that both approximations Eqs. (24) and (28) to a typical river velocity are very accurate and that Dronkers' approach gives the best performance.

Applying Eq. (28) in the same procedure as described in Appendix A for the Lorentz's case, we readily obtain the following expression:

$$\Gamma_{\mathrm{G}} = G_0 + G_1(\mu\lambda)^2\,, \tag{30}$$

with

$$G_0 = \frac{16}{15\pi}\frac{1+2\varphi+7\varphi^2}{1+\varphi}, \qquad G_1 = \frac{32}{15\pi}\frac{1}{1+\varphi}. \tag{31}$$

HESSD
10, 9191–9238, 2013

If $U_r = 0$ (implying that $U' = \upsilon$) $G_0 = 16/(15\pi)$ and $G_1 = 32/(15\pi)$, and the method is identical to Dronkers' expression Eq. (26).

The expression accounting for the periodic variation of the depth in the denominator of the friction term is reported in Table 3, where

$$G_2 = \frac{128}{15\pi}\frac{\varphi}{1+\varphi}, \qquad G_3 = \frac{64}{15\pi}\frac{\frac{1}{3}\varphi + \frac{2}{3}\varphi^2 + \varphi^3}{1+\varphi}. \tag{32}$$

The dependence of the coefficients G_0, G_1, G_2 and G_3 on φ (0–2) is presented in Fig. 3c.

4.5 Hybrid method

Cai et al. (2012a) showed that a linear combination of the traditional Lorentz approach (e.g., Toffolon and Savenije, 2011) with the quasi-nonlinear approach (e.g., Savenije et al., 2008) gives good predictive results. In this study, we expand this method to account for river discharge. Consequently, the new nonlinear friction term reads:

$$F_H = \frac{2}{3}F + \frac{1}{3}F_L = \frac{1}{K^2 h^{4/3}}\left[\frac{2}{3}U|U| + \frac{1}{3}\left(\frac{L_0}{4}\upsilon^2 + \frac{L_1}{2}\upsilon u_t\right)\right], \tag{33}$$

where the subscript H stands for hybrid. Applying the envelope method with this friction formulation, we are able to derive a new river discharge dependent damping equation:

$$\Gamma_H = \frac{2}{3}\Gamma + \frac{1}{3}\Gamma_L, \tag{34}$$

where Γ_L is given by T2 (see Table 3) with $\kappa = 1$, and Γ by either Eq. (14) or (15) in the downstream tide-dominated zone ($\varphi < \mu\lambda$) or in the upstream river discharge-dominated zone ($\varphi \geq \mu\lambda$), respectively.

HESSD
10, 9191–9238, 2013

5 Results

5.1 Analytical solutions of the new models

The different damping equations introduced above should be combined with the phase lag, scaling and celerity equations of Table 2, to form the system of the hydrodynamic equations:

$$\tan(\varepsilon) = \frac{\lambda}{\gamma - \delta}, \tag{35}$$

$$\mu = \frac{\sin(\varepsilon)}{\lambda} = \frac{\cos(\varepsilon)}{\gamma - \delta}, \tag{36}$$

$$\lambda^2 = 1 - \delta(\gamma - \delta). \tag{37}$$

In this way we have a new set of four implicit analytical equations that account for the effect of river discharge. As shown in Savenije et al. (2008), Eqs. (35) and (36) can be combined to eliminate the variable ε to give

$$(\gamma - \delta)^2 = \frac{1}{\mu^2} - \lambda^2. \tag{38}$$

A fully explicit solutions for the main dimensionless parameters (i.e., μ, δ, λ, ε) can be derived in some cases (Toffolon et al., 2006; Savenije et al., 2008), but an iterative procedure is needed to obtain the solution in general. The following procedure usually converges in a few steps: (1) initially we assume $Q_f = 0$ and calculate the initial values for the velocity number μ, celerity number λ and the tidal velocity amplitude υ (and hence dimensionless river discharge term φ) using the analytical solution proposed in Cai et al. (2012a) (see Sect. 3); (2) taking into account the effect of river discharge Q_f, the revised damping number δ, celerity number λ, velocity number μ and velocity amplitude υ (and hence φ) are calculated by solving Eqs. (11), (37) and (38) using a simple Newton–Raphson method; (3) this process is repeated until the result is stable and then the other parameters (e.g., ε, η, υ) are computed.

HESSD
10, 9191–9238, 2013

5.2 Comparison among different approaches

Table 3 summarizes the damping equations with and without the effect of river discharge for the different friction formulations, leading to different forms of the damping equation. The substitution of $\varphi = 0$ yields the same damping equations as in Table 2 (general case), as it can be derived by exploiting the phase lag and scaling equations (Cai et al., 2012a).

As an illustration, the relation between the dependent dimensionless parameters and the dimensionless river discharge φ is shown in Fig. 5 for given values of $\zeta = 0.1$, $\gamma = 1.5$, $\chi = 2$ and $r_S = 1$. We can see that for increasing river discharge all the analytical models approach the same asymptotic solution (except Godin's approach), which is due to the fact that the approximations to the quadratic velocity $U|U|$ is close to U^2 when the effect of tide is less important and the current no longer reverses. Actually, we can see that the parameter Γ in the friction term in T1, T2, T3 and T5 (see Table 3) tends to $(4/3)\zeta\varphi^2/(\mu\lambda)$ when φ approaching infinity, while Godin's approach in T4 tends to $[64/(15\pi)]\zeta\varphi^2/(\mu\lambda)$ (because the quadratic term in G_3 becomes dominant). Moreover, it can be seen from Fig. 5 that the performance of the hybrid model is close to the average of Lorentz's and the quasi-nonlinear method, which is to be expected since the hybrid tidal damping represents a weighted average of these two solutions. In addition, we note that the different methods tend to converge for large values of φ.

It is important to realise that the different approaches use different expressions for the dimensionless friction f (i.e., Eq. 9) as a result of the variation of the depth over time. While the effect of a variable depth is taken into account in the envelope method, the original Lorentz, Dronkers and Godin methods assume a constant depth in the friction term, which is the same as considering $\zeta = 0$ in Eq. (9):

$$f_0 = g/\left(K^2\overline{h}^{-1/3}\right). \tag{39}$$

The damping equations accounting for time variability, which is related to the term ζ in Eq. (9), are presented in Table 3.

HESSD
10, 9191–9238, 2013

5.3 Sensitivity analysis

In this section we discuss the effect of changing the frictional and geometrical features of the estuary. Although in principle all the presented methods can be used, in the following we will consider the hybrid model, if not explicitly mentioned.

The relation between the dependent dimensionless parameters (i.e., the damping number δ, the velocity number μ, the celerity number λ and the phase lag ε) and the friction number χ for different values of φ is shown in Fig. 6 for given values of $\zeta_0 = 0.1$, $\gamma = 1.5$ and $r_S = 1$. In general, the river discharge intensifies the effect of friction, i.e., inducing more tidal damping (hence less velocity amplitude and wave celerity). The phase lag $\varepsilon = \arcsin(\mu\lambda)$ increases with increasing φ except for small χ when the values of $\mu\lambda$ are decreased. However, we can see that the curves show an anomaly for very small value of χ. If χ is very small, the river discharge term in the numerator of the damping Eq. (11) is negligible but becomes important in β, defined in Eq. (12). For this case, an increase of the river discharge has an opposite effect, particularly on the phase lag. In fact, for the case of a frictionless estuary ($\chi = 0$) the damping Eq. (11) reduces to $\delta = \mu^2\gamma\theta/(1+\mu^2\beta)$ in which β is decreased with river discharge.

The friction number χ is also a function of ζ (see Table 1). In order to illustrate the effect of ζ we introduce a modified (time-invariant) friction number χ_0 as:

$$\chi_0 = \chi\left[1-(4\zeta/3)^2\right]/\zeta = r_S g c_0/\left(K^2\omega\overline{h}^{-4/3}\right). \quad (40)$$

Figure 7 describes the effect of the dimensionless tidal amplitude ζ for given values of $\chi_0 = 20$, $\gamma = 1.5$ and $r_S = 1$. Larger ζ intensifies the effect of river discharge and friction as well, which induces more tidal damping, less velocity amplitude and wave celerity, and increases the phase difference between HW and HWS (or LW and LWS). For small value of ζ, the phase lag decreases with increasing river discharge, also due to the effect on β.

Figure 8 shows the effect of the estuary shape number γ on the main dimensionless parameters for different river discharge conditions φ and for given values of the other

HESSD
10, 9191–9238, 2013

independent parameters ($\zeta_0 = 0.1$, $\chi_0 = 20$ and $r_S = 1$). In general, the damping number δ and the velocity number μ decrease with river discharge, which means more tidal damping and less velocity amplitude. On the other hand, the celerity number λ is increased (hence slower wave celerity) due to increasing river discharge. For the phase lag ε, we can see from Fig. 8d that it decreases with river discharge for small values of γ while it increases for larger values of γ. Cai et al. (2012a) found the same relationship between the main dimensionless parameters and the friction number χ, which confirms our point that including river discharge acts in the same way as increasing the friction.

From an analytical point of view, it is easy to show that the influence of river discharge on the tidal dynamics is very similar to that of the friction number χ. Referring for sake of simplicity to the quasi non-linear model and considering an artificial friction number χ_r due to river discharge, the damping Eq. (11) can be written, with Eq. (14) for the case $\varphi < \mu\lambda$, as

$$\delta = \frac{\mu^2}{1+\mu^2\beta}\left[\gamma\theta - (\mu\lambda)^2\chi\left(1 + \frac{8}{3}\zeta\frac{\varphi}{\mu\lambda} + \left(\frac{\varphi}{\mu\lambda}\right)^2\right)\right] = \frac{\mu^2}{1+\mu^2\beta}\left[\gamma\theta - (\mu\lambda)^2\chi_r\right]. \quad (41)$$

This relationship shows that the effect of river discharge is basically that of increasing friction by a factor that is a function of φ. Expressing the artificial friction number as $\chi_r = \chi + \Delta\chi_r$ provides an estimation of the correction of the friction term

$$\frac{\Delta\chi_r}{\chi} = \frac{8}{3}\zeta\frac{\varphi}{\mu\lambda} + \left(\frac{\varphi}{\mu\lambda}\right)^2, \quad (42)$$

which is needed to compensate for the lack of considering river discharge. In fact, increasing φ is analogous to changing χ, and the expected non-physical adjustment of the Manning–Strickler coefficient K can be estimated for models that do not consider Q_f.

HESSD
10, 9191–9238, 2013

5.4 Application to real estuaries

Using the damping Eq. (11) (in the hybrid version, hence $\Gamma = \Gamma_H$), the analytical model has been compared to observations made in the Modaomen and Yangtze estuaries in China, where the influence of river discharge in the upstream part is considerable. The Modaomen estuary forms the downstream part of the West River entering the Pearl River Delta with an annual river discharge of $7115\,m^3\,s^{-1}$ at Makou (Cai et al., 2012b). The Yangtze estuary drains the Yangtze River basin with an annual mean river discharge of $28\,310\,m^3\,s^{-1}$ at Datong (Zhang et al., 2012).

The computation depends on the three independent variables, i.e., γ, χ_0 and φ. Given the flow boundary conditions (i.e., the tidal amplitude at the seaward boundary and river discharge at the landward boundary) and the geometry of the channel, the values of γ, χ_0 and φ can be computed. Hence, the set of four implicit analytical Eqs. (11) (with $\Gamma = \Gamma_H$), (35), (36) and (37) can be solved by simple iteration. The tidal amplitude is obtained by numerical integration of the damping number δ over a length step (e.g., 1 km).

Table 4 presents the geometry and flow characteristics (considering two different cases for independent calibration and verification of the model) of the Modaomen and Yangtze on which the computations are based. The convergence length of the cross-sectional area, which is the length scale of the exponential function, is obtained by fitting Eq. (1), where the parallel branches separated by islands are combined, as recommended by Nguyen and Savenije (2006) and Zhang et al. (2012). The calibrated parameters including the storage width ratio r_S and the Manning–Strickler friction K are presented in Table 5. In general, the storage width ratio r_S ranges between 1 and 2 (Savenije, 2005, 2012). It is noted that a relatively small roughness value of $K = 70$–$75\,m^{1/3}\,s^{-1}$ (Table 5) was used in the Yangtze estuary, which is due to the fact that it is a silt-mud estuary, while the bed consists of sands in the Modaomen estuary. The reason for a small roughness value of $K = 78\,m^{1/3}\,s^{-1}$ used in the middle reach of the

HESSD
10, 9191–9238, 2013

Modaomen estuary (43–91 km) is probably due to the effect of parallel branches (see Cai et al., 2012b).

Figure 9 shows the longitudinal computation of the tidal amplitude, the travel time (both at HW and LW) and damping number applied to the Modaomen estuary. Observations of tidal amplitude and travel time of the tidal wave on 8–9 February 2001 were used to calibrate the model, while the observed data on 5–6 December 2002 were used for verification. Both the model with river discharge and the model without river discharge can be made to fit the observations if a suitable friction coefficient is used, as discussed in the previous section. However, such calibrations yield significantly lower values of the Manning–Strickler coefficients upstream. For the model without river discharge we would have required an unrealistically low Manning–Strickler value of $K = 30\,\mathrm{m}^{1/3}\,\mathrm{s}^{-1}$ to fit the data in the upstream part of Modaomen estuary (91–150 km). In Fig. 9, the new model accounting for the effect of river discharge is compared to the original model with the same roughness, but without river discharge. In the lower part of the estuary the models behave the same (e.g., see the dimensionless damping number in Fig. 9c, f), but behave differently in the upper reach where the river discharge is dominant. Without considering river discharge, the model underestimates tidal damping upstream.

In Fig. 10, we can see that the analytically calculated tidal amplitude in the Yangtze estuary is in good correspondence with the observed data on 21–22 December 2006 (calibration) and 18–19 February 2003 (verification). For the travel time, the correspondence with observations at HW is very good, but the correspondence for LW shows a big deviation from the measurements, with an underestimation of the celerity for LW. The reason for the deviation should probably be attributed to significant tidal wave distortion due to the strong river discharge, which is critical for the assumption that the celerities at HW and LW times are symmetrical compared with the tidal average wave celerity (see Eq. A8 in Appendix A). Without considering the river discharge, a much higher and unrealistic roughness (implying a lower value of $K = 26\,\mathrm{m}^{1/3}\,\mathrm{s}^{-1}$) would be

HESSD
10, 9191–9238, 2013

necessary in the upstream part of the estuary (275–600 km) to compensate the influence of river discharge.

5.5 A new approach for estimating river discharge

Reliable estimation of river discharge into estuaries is a critical component of water resources management (e.g., salt intrusion, freshwater withdrawal, flood protection etc.), yet river discharge into estuaries remains poorly observed, as it requires observations during a full tidal cycle. The analytical model for tidal wave propagation makes clear that tide and river discharge interact and are governed by the damping Eq. (11). As a result, it is possible to develop an analytical equation to estimate river discharge based on measurements of tidal water levels. If the tidal damping δ is known, we can use one of the described methods to predict river discharge. In the following analysis, we will refer to the hybrid method.

Knowing δ and γ, the tidal variables ε, λ and μ can be determined using Eqs. (35), (37) and (38). In the seaward part of the estuary, the effect of river discharge on tidal dynamics is usually negligible. Making use of this phenomenon it is possible to determine the time-invariant friction number χ_0 (defined by Eq. 40) using the hybrid model without river discharge (see Sect. 3) by calibrating on the tidal observations in the tide-dominated zone. Subsequently the damping Eq. (11) (referring to the hybrid method, hence with $\Gamma = \Gamma_H$) is used in the upstream river discharge-dominated zone ($\varphi \geq \mu\lambda$) to predict the river discharge. Recalling that $L_0 = -2 - 4\varphi^2$, $L_1 = 4\varphi$ for the case of $\varphi \geq 1$ and rearranging Eq. (11), it is possible to obtain a quadratic equation of φ:

$$\alpha_1\varphi^2 + \alpha_2\varphi + \alpha_3 = 0\,, \tag{43}$$

with

HESSD
10, 9191–9238, 2013

$$\alpha_1 = \frac{4}{3}\mu^2\chi\zeta\,,$$
$$\alpha_2 = \frac{\mu}{\lambda}\left[-r_S\zeta\delta + 2\chi\mu^2\lambda^2 + (\gamma-\delta)\left(\sqrt{1+\zeta}-1\right)\right],$$
$$\alpha_3 = \delta + \mu^2\left[-(\gamma-\delta) + \frac{2}{9}\chi\zeta\left(1+4\mu^2\lambda^2\right)\right], \quad (44)$$

where $\chi = \chi_0\zeta\left[1-\left(4\zeta/3\right)^2\right]^{-1}$ is calculated with the local value of ζ.

For given values of δ, γ, λ, μ, χ_0 and ζ, the positive solution is:

$$\varphi = \frac{-\alpha_2 + \sqrt{\alpha_2^2 - 4\alpha_1\alpha_3}}{2\alpha_1}. \quad (45)$$

With this solution for φ, an explicit solution is obtained for $Q_f = \overline{A}\,U_r = \overline{A}\varphi\upsilon$.

As an example, Fig. 11 shows estimates of the river discharge Q_f over a range of values of δ (−2–0) at x = 116 km in the Modaomen estuary and x = 372 km in the Yangtze estuary located between the two points where tidal observations can be obtained.

We see from Fig. 11 that the river discharge is almost linearly proportional to the tidal damping. The correspondence with observations is good, which suggests that the proposed analytical model can be a useful tool to have a first order estimation of river discharge in the tidal region. Further work will be required to test the accuracy of the explicit Eq. (45).

6 Conclusions

In this paper, we have extended the analytical framework for tidal hydrodynamics proposed by Cai et al. (2012a) by taking account of river discharge. With the envelope

HESSD
10, 9191–9238, 2013

method (Savenije, 1998), different friction formulations considering river discharge can be used to derive expressions for the envelopes at HW and LW and subsequently to arrive at the corresponding damping equations. When combined with the phase lag equation, the scaling equation and the celerity equation, these damping equations can be iteratively solved for the dimensionless parameters μ, δ, λ and ε, which are related to tidal velocity amplitude, tidal damping, wave celerity, and phase lag, respectively. Thus, for given topography, friction, tidal amplitude at the seaward boundary and river discharge at the landward boundary, we can reproduce the main tidal dynamics along the estuary.

Unlike previous studies (e.g., Godin, 1985, 1999) that neglect higher-order term, the envelope method retains all terms although it still requires a small tidal amplitude to depth ratio. This allows for including river discharge in a fully analytical framework. It is also worth recognising that the friction term has two nonlinear sources, the quadratic velocity $U|U|$, and the variation of the hydraulic radius (approximated by the flow depth h) in the denominator (Parker, 1991). Lorentz's, Dronkers' and Godin's friction formulations disregarded the tidally varying depth and only focus on the quadratic velocity. By using the envelope method, we are able to take this second nonlinear source into account and end up with a more complete damping equation accounting for river discharge.

With respect to e.g. Cai et al. (2012a), where we did not consider the effect of river discharge, this method is an improvement that is important especially in the upstream part of the estuary where the influence of river discharge is considerable. This is clearly demonstrated by the application of the analytical model to two real estuaries (Modaomen and Yangtze in China), which shows that the proposed model fits the observations with realistic roughness value in the upstream part, while the model without considering river discharge can only be fitted with unrealistically high roughness values. Furthermore, the proposed damping equation has the potential for estimating river discharge in estuaries on the basis of tidal water level observations, which are easy to obtain in practice.

HESSD
10, 9191–9238, 2013

Appendix A

Derivation of Lorentz's damping equation incorporating river discharge using the envelope method

Using a Lagrangean approach as in Savenije (2005, 2012), the continuity equation can be written as:

$$\frac{\mathrm{d}V}{\mathrm{d}t} = r_\mathrm{s}\frac{c}{h}\frac{\mathrm{d}h}{\mathrm{d}t} - \frac{cV}{b} + cV\frac{1}{\eta}\frac{\mathrm{d}\eta}{\mathrm{d}x}. \tag{A1}$$

The momentum equation can also be written in a Lagrangean form, yielding:

$$\frac{\mathrm{d}V}{\mathrm{d}t} + g\frac{\partial h}{\partial x} + g\left(I_\mathrm{b} - I_r\right) + g\frac{V|V|}{K^2h^{4/3}} = 0, \tag{A2}$$

where I_b is the bottom slope and I_r is the water level residual slope resulting from the density gradient. Combination of these equations, and using $V = \mathrm{d}x/\mathrm{d}t$, yields:

$$r_\mathrm{s}\frac{cV}{gh}\frac{\mathrm{d}h}{\mathrm{d}x} - \frac{cV}{g}\left(\frac{1}{b} - \frac{1}{\eta}\frac{\mathrm{d}\eta}{\mathrm{d}x}\right) + \frac{\partial h}{\partial x} + I_\mathrm{b} - I_r + \frac{V|V|}{K^2h^{4/3}} = 0. \tag{A3}$$

Next, we condition Eq. (A3) for the situation of high water (HW) and low water (LW). The following relations apply to h_HW and h_LW:

$$\frac{\mathrm{d}h_\mathrm{HW}}{\mathrm{d}x} - \frac{\mathrm{d}h_\mathrm{LW}}{\mathrm{d}x} = 2\frac{\mathrm{d}\eta}{\mathrm{d}x}, \tag{A4}$$

$$\frac{\mathrm{d}h_\mathrm{HW,LW}}{\mathrm{d}x} = \left.\frac{\partial h}{\partial x}\right|_\mathrm{HW,LW}, \tag{A5}$$

$$\frac{\mathrm{d}h_\mathrm{HW}}{\mathrm{d}x} + \frac{\mathrm{d}h_\mathrm{LW}}{\mathrm{d}x} \approx 2\frac{\mathrm{d}\bar{h}}{\mathrm{d}x}, \tag{A6}$$

HESSD
10, 9191–9238, 2013

with $h_{HW} \approx \overline{h} + \eta$ and $h_{LW} \approx \overline{h} - \eta$. These three equations are acceptable if $\eta/\overline{h} \ll 1$.

The tidal velocities at HW and LW the following expressions can be expressed as

$$V_{HW} \approx \upsilon \sin(\varepsilon) - U_r, \qquad V_{LW} \approx -\upsilon \sin(\varepsilon) - U_r, \tag{A7}$$

where the river flow velocity U_r is negative (it is in ebb direction). Further we assume that wave celerity is proportional to the square root of the depth:

$$\frac{c_{HW}}{\sqrt{h_{HW}}} \approx \frac{c_{LW}}{\sqrt{h_{LW}}} \approx \frac{c}{\sqrt{\overline{h}}}, \tag{A8}$$

In this example we use Lorentz's linearization Eq. (21) of the bed friction (Lorentz, 1926), but also take into account the effect of the periodic variation of the hydraulic radius in the denominator of the friction term (i.e., $K^2 h^{4/3}$). Combination of Eqs. (A3), (A5), and the first of Eq. (A7) yields the following envelope for HW:

$$\frac{r_s c_{HW}[\upsilon \sin(\varepsilon) - U_r]}{g\left(\overline{h} + \eta\right)} \frac{\mathrm{d}h_{HW}}{\mathrm{d}x} - \frac{c_{HW}[\upsilon \sin(\varepsilon) - U_r]}{g}\left(\frac{1}{b} - \frac{1}{\eta}\frac{\mathrm{d}\eta}{\mathrm{d}x}\right) + \frac{\mathrm{d}h_{HW}}{\mathrm{d}x}$$
$$+ \frac{1}{K^2\left(\overline{h} + \kappa\eta\right)^{4/3}}\left[\frac{1}{4}L_0\upsilon^2 + \frac{1}{2}L_1\upsilon^2 \sin(\varepsilon)\right] = -I_b + I_r \tag{A9}$$

where $\kappa = 1$ corresponds to the time-dependent case, while $\kappa = 0$ to the time-independent case. Similarly, for LW, combination of Eqs. (A3), (A5), and the second of Eq. (A7) yields the LW envelope:

$$-\frac{r_s c_{LW}[\upsilon \sin(\varepsilon) + U_r]}{g\left(\overline{h} - \eta\right)} \frac{\mathrm{d}h_{LW}}{\mathrm{d}x} + \frac{c_{LW}[\upsilon \sin(\varepsilon) + U_r]}{g}\left(\frac{1}{b} - \frac{1}{\eta}\frac{\mathrm{d}\eta}{\mathrm{d}x}\right) + \frac{\mathrm{d}h_{LW}}{\mathrm{d}x}$$
$$+ \frac{1}{K^2\left(\overline{h} - \kappa\eta\right)^{4/3}}\left[\frac{1}{4}L_0\upsilon^2 - \frac{1}{2}L_1\upsilon^2 \sin(\varepsilon)\right] = -I_b + I_r \tag{A10}$$

HESSD
10, 9191–9238, 2013

Subtraction of these envelopes, using a Taylor series expansion of $h^{4/3}$, and taking into account the assumption on the wave celerity yields the following expressions:

$$\frac{r_S c\upsilon \sin(\varepsilon)}{\overline{h}}\left(\frac{1}{\sqrt{1+\zeta}}\frac{\mathrm{d}h_{HW}}{\mathrm{d}x}+\frac{1}{\sqrt{1-\zeta}}\frac{\mathrm{d}h_{LW}}{\mathrm{d}x}\right)$$
$$-\frac{r_S cU_r}{\overline{h}}\left(\frac{1}{\sqrt{1+\zeta}}\frac{\mathrm{d}h_{HW}}{\mathrm{d}x}-\frac{1}{\sqrt{1-\zeta}}\frac{\mathrm{d}h_{LW}}{\mathrm{d}x}\right)$$
$$-\left[2c\upsilon\sin(\varepsilon)+2cU_r\left(1-\sqrt{1+\zeta}\right)\right]\left(\frac{1}{b}-\frac{1}{\eta}\frac{\mathrm{d}\eta}{\mathrm{d}x}\right)$$
$$+2g\frac{\mathrm{d}\eta}{\mathrm{d}x}+f'\left[\frac{L_1\upsilon^2\sin(\varepsilon)}{\overline{h}}-\kappa\frac{2L_0\upsilon^2\zeta}{3\overline{h}}\right]=0 \quad \text{(A11)}$$

with the dimensionless friction factor f' defined as

$$f'=g/\left(K^2\overline{h}^{1/3}\right)\left[1-\left(\kappa 4\zeta/3\right)^2\right]^{-1}. \quad \text{(A12)}$$

The parts between brackets in the first and second terms of Eq. (A11) can be replaced by the residual water level slope $\mathrm{d}\overline{h}/\mathrm{d}x$ defined in Eq. (A6) and $\mathrm{d}\overline{h}/\mathrm{d}x$ defined in Eq. (A4), respectively, provided $\zeta \ll 1$. Elaboration yields:

$$\frac{1}{\eta}\frac{\mathrm{d}\eta}{\mathrm{d}x}\left(\theta-r_s\frac{\varphi}{\sin(\varepsilon)}\zeta+\frac{g\eta}{c\upsilon\sin(\varepsilon)}\right)=\frac{\theta}{b}-r_s\frac{1}{\overline{h}}\frac{\mathrm{d}\overline{h}}{\mathrm{d}x}$$
$$-\frac{L_1}{2}f'\frac{\upsilon}{\overline{h}c}+\kappa\frac{L_0}{3}f'\frac{\upsilon\zeta}{\overline{h}c}\frac{1}{\sin(\varepsilon)} \quad \text{(A13)}$$

The dimensionless parameters φ and θ have been defined in the main text. The first two terms on the right hand side of Eq. (A13) represent the width and depth conver-

HESSD
10, 9191–9238, 2013

gences and can be written as:

$$\frac{\theta}{b} - r_S \frac{1}{\bar{h}} \frac{d\bar{h}}{dx} = \frac{\theta}{b} + \frac{r_S}{d} \approx \frac{\theta}{a}. \tag{A14}$$

Here, it has been assumed that both θ and r_S are close to unity. Substitution of Eq. (A14) into (A13) yields

$$\frac{1}{\eta}\frac{d\eta}{dx}\left(\theta - r_s \frac{\varphi}{\sin(\varepsilon)}\zeta + \frac{g\eta}{c\upsilon\sin(\varepsilon)}\right) = \frac{\theta}{a} - \frac{L_1}{2} f' \frac{\upsilon}{\bar{h}c} + \kappa \frac{L_0}{3} f' \frac{\upsilon\zeta}{\bar{h}c} \frac{1}{\sin(\varepsilon)} \tag{A15}$$

Making use of the dimensionless parameters and adopting the scaling equation $\sin(\varepsilon) = \mu\lambda$, Eq. (A15) reduces to the following expression:

$$\delta = \frac{\mu^2}{1 + \mu^2\left[\theta - r_s\varphi\zeta/(\mu\lambda)\right]}\left[\gamma\theta - \chi\left(\frac{1}{2}L_1\mu\lambda - \kappa\frac{1}{3}L_0\zeta\right)\right], \tag{A16}$$

or

$$\delta = \frac{\mu^2}{1+\mu^2\beta}(\gamma\theta - \chi\mu\lambda\Gamma_L), \quad \Gamma_L = \frac{L_1}{2} - \kappa\zeta\frac{L_0}{3\mu\lambda}. \tag{A17}$$

The notation used in this paper is presented in Table A1.

Acknowledgements. The first author is financially supported for his Ph.D. research by the China Scholarship Council with the project reference number of 2010638037.

HESSD
10, 9191–9238, 2013

References

Cai, H., Savenije, H. H. G., and Toffolon, M.: A new analytical framework for assessing the effect of sea-level rise and dredging on tidal damping in estuaries, J. Geophys. Res., 117, C09023, doi:10.1029/2012JC008000, 2012a. 9193, 9194, 9196, 9197, 9198, 9204, 9205, 9206, 9208, 9212, 9213, 9222, 9223

Cai, H., Savenije, H. H. G., Yang, Q., Ou, S., and Lei, Y.: Influence of river discharge and dredging on tidal wave propagation: modaomen estuary case, J. Hydraul. Eng.-ASCE, 138, 885–896, doi:10.1061/(ASCE)HY.1943-7900.0000594, 2012b. 9192, 9193, 9199, 9209, 9210, 9223

Dronkers, J. J.: Tidal computations in River and Coastal Waters, Elsevier, New York, 1964. 9193, 9198, 9200, 9201, 9202, 9223

Friedrichs, C. T. and Aubrey, D. G.: Tidal propagation in strongly convergent channels, J. Geophys. Res., 99, 3321–3336, 1994. 9193

Godin, G.: Modification of river tides by the discharge, J. Waterw. Port C. Div., 111, 257–274, 1985. 9193, 9213

Godin, G.: Compact approximations to the bottom friction term, for the study of tides propagating in channels, Cont. Shelf. Res., 11, 579–589, 1991. 9193, 9203, 9223

Godin, G.: The propagation of tides up rivers with special considerations on the upper Saint Lawrence river, Estuar. Coast. Shelf S., 48, 307–324, 1999. 9193, 9203, 9213, 9223

Horrevoets, A. C., Savenije, H. H. G., Schuurman, J. N., and Graas, S.: The influence of river discharge on tidal damping in alluvial estuaries, J. Hydrol., 294, 213–228, 2004. 9193, 9199, 9223

Hunt, J. N.: Tidal oscillations in estuaries, Geophys. J. Roy. Astr. S., 8, 440–455, 1964. 9193

Ippen, A. T. (Ed.): Tidal dynamics in estuaries, Part 1: Estuaries of rectangular section, in: Estuary and Coastline Hydrodynamics, 493–522, McGraw-Hill, New York, 1966. 9193

Jay, D. A.: Green law revisited – tidal long-wave propagation in channels with strong topography, J. Geophys. Res., 96, 20585–20598, 1991. 9193

Jay, D. A., Leffler, K., and Degens, S.: Long-Term Evolution of Columbia River Tides, J. Waterw. Port C. Div., 137, 182–191, 2011. 9193

Kukulka, T. and Jay, D. A.: Impacts of Columbia River discharge on salmonid habitat: 1. A nonstationary fluvial tide model, J. Geophys. Res., 108, 3293, doi:10.1029/2002JC001382, 2003. 9193

HESSD
10, 9191–9238, 2013

Lanzoni, S. and Seminara, G.: On tide propagation in convergent estuaries, J. Geophys. Res., 103, 30793–30812, 1998. 9193

Leblond, P. H.: Tidal propagation in Shallow Rivers, J. Geophys. Res., 83, 4717–4721, 1978. 9193

Lorentz, H. A.: Verslag Staatscommissie Zuiderzee, Algemene Landsdrukkerij, The Hague, Netherlands, 1926 (in Dutch). 9193, 9198, 9215, 9223

Nguyen, A. D. and Savenije, H. H.: Salt intrusion in multi-channel estuaries: a case study in the Mekong Delta, Vietnam, Hydrol. Earth Syst. Sci., 10, 743–754, doi:10.5194/hess-10-743-2006, 2006. 9209

Parker, B. B. (Ed.): The relative importance of the various nonlinear mechanisms in a wide range of tidal interactions, in: Tidal Hydrodynamics, 236–268, John Wiley, New York, 1991. 9193, 9213

Prandle, D.: Relationships between tidal dynamics and bathymetry in strongly convergent estuaries, J. Phys. Oceanogr., 33, 2738–2750, 2003. 9193

Savenije, H. H. G.: Lagrangian solution of St Venants equations for alluvial estuary, J. Hydraul. Eng.-ASCE, 118, 1153–1163, 1992. 9194, 9197

Savenije, H. H. G.: Determination of estuary parameters on basis of lagrangian analysis, J. Hydraul. Eng.-ASCE, 119, 628–642, 1993. 9197

Savenije, H. H. G.: Analytical expression for tidal damping in alluvial estuaries, J. Hydraul. Eng.-ASCE, 124, 615–618, 1998. 9193, 9197, 9213, 9223

Savenije, H. H. G.: A simple analytical expression to describe tidal damping or amplification, J. Hydrol., 243, 205–215, 2001. 9193, 9197

Savenije, H. H. G.: Salinity and Tides in Alluvial Estuaries, Elsevier, New York, 2005. 9195, 9209, 9214

Savenije, H. H. G.: Salinity and Tides in Alluvial Estuaries, completely revised 2nd Edn., available at: www.salinityandtides.com (last access: 26 June 2013), 2012. 9195, 9209, 9214

Savenije, H. H. G. and Veling, E. J. M.: Relation between tidal damping and wave celerity in estuaries, J. Geophys. Res., 110, C04007, doi:10.1029/2004JC002278, 2005. 9197

Savenije, H. H. G., Toffolon, M., Haas, J., and Veling, E. J. M.: Analytical description of tidal dynamics in convergent estuaries, J. Geophys. Res., 113, C10025, doi:10.1029/2007JC004408, 2008. 9193, 9196, 9197, 9198, 9199, 9204, 9205, 9223, 9228

Toffolon, M. and Savenije, H. H. G.: Revisiting linearized one-dimensional tidal propagation, J. Geophys. Res., 116, C07007, doi:10.1029/2010JC006616, 2011. 9193, 9196, 9204

HESSD

10, 9191–9238, 2013

Toffolon, M., Vignoli, G., and Tubino, M.: Relevant parameters and finite amplitude effects in estuarine hydrodynamics, J. Geophys. Res., 111, C10014, doi:10.1029/2005JC003104, 2006. 9196, 9197, 9205

Van Rijn, L. C.: Analytical and numerical analysis of tides and salinities in estuaries; Part 1: Tidal wave propagation in convergent estuaries, Ocean Dynam., 61, 1719–1741, doi:10.1007/s10236-011-0453-0, 2011. 9193

Zhang, E. F., Savenije, H. H. G., Wu, H., Kong, Y. Z., and Zhu, J. R.: Analytical solution for salt intrusion in the Yangtze Estuary, China, Estuar. Coast. Shelf S., 91, 492–501, 2011. 9192

Zhang, E. F., Savenije, H. H. G., Chen, S. L., and Mao, X. H.: An analytical solution for tidal propagation in the Yangtze Estuary, China, Hydrol. Earth Syst. Sci., 16, 3327–3339, doi:10.5194/hess-16-3327-2012, 2012. 9192, 9209

HESSD
10, 9191–9238, 2013

Table 1. The definition of dimensionless parameters.

Dimensionless parameters	
Independent	Dependent
	Damping number $\delta = c_0 \mathrm{d}\zeta/(\zeta\omega \mathrm{d}x)$
Tidal amplitude at the downstream boundary $\zeta_0 = \eta_0/\overline{h}$	Velocity number $\mu = \upsilon/(r_S\zeta c_0) = \upsilon\overline{h}/(r_S\eta c_0)$
Estuary shape number $\gamma = c_0/(\omega a)$	Celerity number $\lambda = c_0/c$
Reference friction number $\chi_0 = r_S g c_0/(K^2\omega\overline{h}^{4/3})$	Phase lag $\varepsilon = \pi/2 - (\phi_z - \phi_U)$
	Tidal amplitude $\zeta = \eta/\overline{h}$
	Friction number $\chi = \chi_0\zeta\left[1 - (4\zeta/3)^2\right]^{-1} = r_S f c_0 \zeta/\left(\omega\overline{h}\right)$

HESSD
10, 9191–9238, 2013

Table 2. Analytical framework for tidal wave propagation (Cai et al., 2012a).

Case		Phase lag $\tan(\varepsilon)$	Scaling μ	Celerity λ^2	Damping δ
General	Quasi-nonlinear	$\lambda/(\gamma-\delta)$	$\cos(\varepsilon)/(\gamma-\delta)$	$1-\delta(\gamma-\delta)$	$\gamma/2-\chi\mu^2/2$
	Linear				$\gamma/2-4\chi\mu/(3\pi\lambda)$
	Dronkers				$\gamma/2-8\chi\mu/(15\pi\lambda)-16\chi\mu^3\lambda/(15\pi)$
	Hybrid				$\gamma/2-4\chi\mu^2/(9\pi\lambda)-\chi\mu^2/3$
Constant cross-section	Quasi-nonlinear	$-\lambda/\delta$	$-\cos(\varepsilon)/\delta$	$1+\delta^2$	$-\chi\mu^2/2$
	Linear				$-4\chi\mu/(3\pi\lambda)$
	Dronkers				$-8\chi\mu/(15\pi\lambda)-16\chi\mu^3\lambda/(15\pi)$
	Hybrid				$-4\chi\mu^2/(9\pi\lambda)-\chi\mu^2/3$
Frictionless ($\gamma<2$)		$\sqrt{4/\gamma^2-1}$	1	$1-\gamma^2/4$	$\gamma/2$
Frictionless ($\gamma\geq 2$)		0	$(\gamma-\sqrt{\gamma^2-4})/2$	0	$(\gamma-\sqrt{\gamma^2-4})/2$
Ideal estuary		$1/\gamma$	$\sqrt{1/(1+\gamma^2)}$	1	0

HESSD
10, 9191–9238, 2013

Table 3. Comparison of the terms in the damping Eq. (11) for different analytical methods. The effect of the time-dependent depth in the friction term for Lorentz's, Dronkers' and Godin's method is accounted for by setting $\kappa=1$ in the expressions for Γ, whereas $\kappa=0$ describes the time-independent case.

Model	Friction term	Γ without river discharge ($\varphi = 0$)	Γ with river discharge ($\varphi > 0$), introducing $\psi = \varphi/(\mu\lambda)$	
Savenije[a,b,c,d]	$\frac{U\lvert U\rvert}{K^2 h^{4/3}}$	$\mu\lambda$	$\begin{cases} \mu\lambda\left(1+\frac{8}{3}\zeta\psi+\psi^2\right) & (\psi<1) \\ \mu\lambda\left(\frac{4}{3}\zeta+2\psi+\frac{4}{3}\zeta\psi^2\right) & (\psi\geq 1) \end{cases}$	T1
Lorentz[e]	$\frac{1}{K^2 h^{4/3}}\left(\frac{L_0}{4}\upsilon^2+\frac{L_1}{2}\upsilon U_t\right)$	$8/(3\pi)$	$\frac{L_1}{2}-\kappa\zeta\frac{L_0}{3\mu\lambda}$	T2
Dronkers[f]	$\frac{1}{K^2 h^{4/3}}(p_0\upsilon^2+p_1\upsilon U+p_2U^2+p_3U^3/\upsilon)$	$\frac{16}{15\pi}+\frac{32}{15\pi}(\mu\lambda)^2$	$\frac{1}{\pi}\Big\{-p_0\frac{4\kappa\zeta}{3\mu\lambda}+p_1\left(1+\frac{4}{3}\kappa\zeta\psi\right)$ $-2p_2\varphi\left[1+\frac{2}{3}\kappa\zeta\left(\frac{1}{\psi}+\psi\right)\right]$ $+p_3\varphi^2\left[3+\frac{1}{\psi^2}+4\kappa\zeta\left(\frac{1}{\psi}+\frac{\psi}{3}\right)\right]\Big\}$	T3
Godin[g]	$\frac{16}{15\pi}\frac{U'^2}{K^2 h^{4/3}}\left[\frac{U}{U'}+2\left(\frac{U}{U'}\right)^3\right]$	$\frac{16}{15\pi}+\frac{32}{15\pi}(\mu\lambda)^2$	$G_0+G_1(\mu\lambda)^2+\kappa\zeta\left(G_2\mu\lambda+\frac{G_3}{\mu\lambda}\right)$	T4
Hybrid[h]	$\frac{2}{3}\frac{U\lvert U\rvert}{K^2 h^{4/3}}+\frac{1}{3}\frac{1}{K^2 h^{4/3}}\left(\frac{L_0}{4}\upsilon^2+\frac{L_1}{2}\upsilon U_t\right)$	$\frac{2}{3}\mu\lambda+\frac{8}{9\pi}$	$\begin{cases} \frac{2}{3}\mu\lambda\left(1+\frac{8}{3}\zeta\psi+\psi^2\right)+\frac{L_1}{6}-\frac{L_0}{9}\frac{\zeta}{\mu\lambda} & (\psi<1) \\ \frac{2}{3}\mu\lambda\left(\frac{4}{3}\zeta+2\psi+\frac{4}{3}\zeta\psi^2\right)+\frac{L_1}{6}-\frac{L_0}{9}\frac{\zeta}{\mu\lambda} & (\psi\geq 1) \end{cases}$	T5
		$\beta=1, \quad \theta=1$	$\beta=\theta-r_S\zeta\psi, \quad \theta\approx 1$	

[a] Savenije (1998); [b] Horrevoets et al. (2004); [c] Savenije et al. (2008); [d] Cai et al. (2012b); [e] Lorentz (1926); [f] Dronkers (1964); [g] Godin (1991, 1999); [h] Cai et al. (2012a)

HESSD
10, 9191–9238, 2013

Table 4. Geometric and flow characteristics of the estuaries studied.

Estuary	Reach (km)	Depth $\overline{h}$ (m)	Convergence length a (km)	Tidal amplitude at the mouth (m)		River discharge Q_f ($m^3 s^{-1}$)	
				Calibration	Verification	Calibration	Verification
Modaomen	0–43	6.3	106	1.31	1.09	2259	2570
	43–91	7	infinite				
	91–150	10.3	110				
Yangtze	0–34	7	42	1.8	2.3	13 100	17 600
	34–275	9	140				
	275–600	11	200				

HESSD
10, 9191–9238, 2013

Table 5. Calibrated parameters of the estuaries studied.

Estuary	Reach (km)	Storage width ratio r_S (–)	Manning–Strickler friction K ($m^{1/3}s^{-1}$), $Q_f > 0$
Modaomen	0–43	1.5	48
	43–91	1.4	78
	91–150	1.3	38
Yangtze	0–34	1.8	70
	34–275	1	75
	275–600	1	70

HESSD
10, 9191–9238, 2013

Table A1. Nomenclature.

The following symbols are used in this paper:	
a	convergence length of cross-sectional area;
$\overline{A}$	tidally averaged cross-sectional area of flow;
$\overline{A_0}$	tidally averaged cross-sectional area at the estuary mouth;
b	convergence length of width;
$\overline{B}$	stream width;
$\overline{B_0}$	tidally averaged width at the estuary mouth;
B_s	storage width;
c	wave celerity;
c_0	celerity of a frictionless wave in a prismatic channel;
c_{HW}	wave celerity at HW;
c_{LW}	wave celerity at LW;
d	convergence length of depth;
f	friction factor accounting for the difference in friction at HW and LW;
f_0	friction factor without considering the difference in friction at HW and LW;
F	quadratic friction term;
F_D	Dronkers' friction term accounting for river discharge;
F_G	Godin's friction term accounting for river discharge;
F_H	Hybrid friction term accounting for river discharge;
F_L	Lorentz's friction term accounting for river discharge;
g	acceleration due to gravity;
G_0, G_1, G_2, G_3	Godin's coefficients accounting for river discharge;
h	cross-sectional average depth;
$\overline{h}$	tidal average depth;
$\overline{h_0}$	tidally averaged depth at the estuary mouth;
h_{HW}	depth at HW;
h_{LW}	depth at LW;
I_b	bottom slope;
I_r	water level residual slope due to the density gradient;
K	Manning–Strickler friction factor;

HESSD
10, 9191–9238, 2013

Table A1. Continued.

The following symbols are used in this paper:	
L_0, L_1	Lorentz's coefficients accounting for river discharge;
p_0, p_1, p_2, p_3	Chebyschev coefficients accounting for river discharge;
Q_f	river discharge;
r_s	storage width ratio;
t	time;
T	tidal period;
U	cross-sectional average flow velocity;
U_t	tidal velocity;
U_r	river velocity;
U'	the maximum possible velocity in Godin's approach;
V_{HW}	velocity at HW;
V_{LW}	velocity at LW;
V	Lagrangean velocity for a moving particle;
x	distance;
z	free surface elevation;
α, β	functions of dimensionless river discharge term φ;
γ	estuary shape number;
Γ	damping parameter of quasi-nonlinear model;
Γ_L	damping parameter of linear model;
Γ_D	damping parameter of Dronkers' model;
Γ_G	damping parameter of Godin's model;
Γ_H	damping parameter of hybrid model;
δ	damping number;
ε	phase lag between HW and HWS (or LW and LWS);
ζ	tidal amplitude to depth ratio;
η	tidal amplitude;
η_0	tidal amplitude at the estuary mouth;
θ	dimensionless term accounting for wave celerity not being equal at HW and LW;
κ	coefficient that include the effect of time-dependent depth in the friction term;
λ	celerity number;
μ	velocity number;
ρ	water density;
υ	tidal velocity amplitude;
ϕ_z, ϕ_U	phase of water level and velocity;
φ	dimensionless river discharge term accounting for river discharge;
χ	friction number;
χ_0	time-invariant friction number;
ω	tidal frequency.

HESSD
10, 9191–9238, 2013

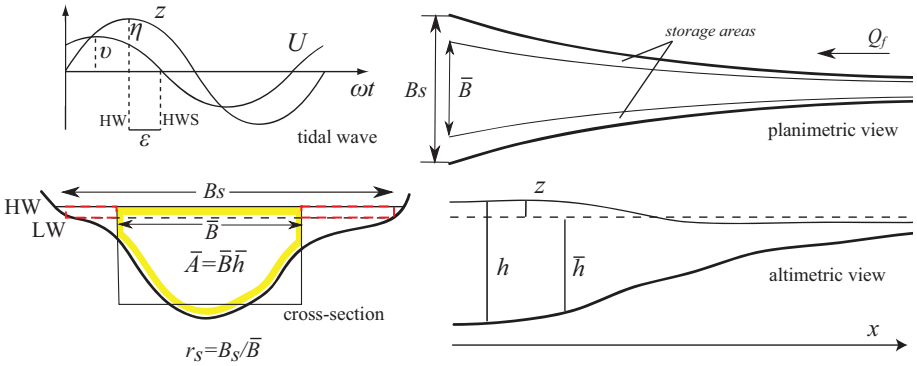

Fig. 1. Sketch of the estuary geometry and basic notations (after Savenije et al., 2008).

HESSD
10, 9191–9238, 2013

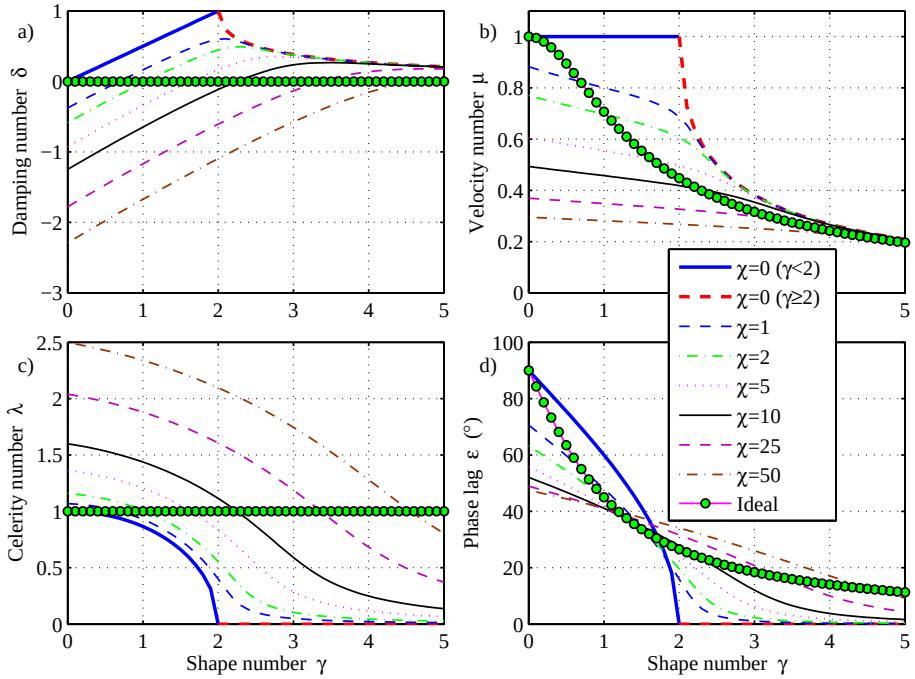

Fig. 2. Variation of damping number δ, the velocity number μ, celerity number λ and phase lag ε with the estuary shape number γ for different values of the friction number χ, obtained with the hybrid model. The green symbols represent the ideal estuary (see Table 2).

HESSD
10, 9191–9238, 2013

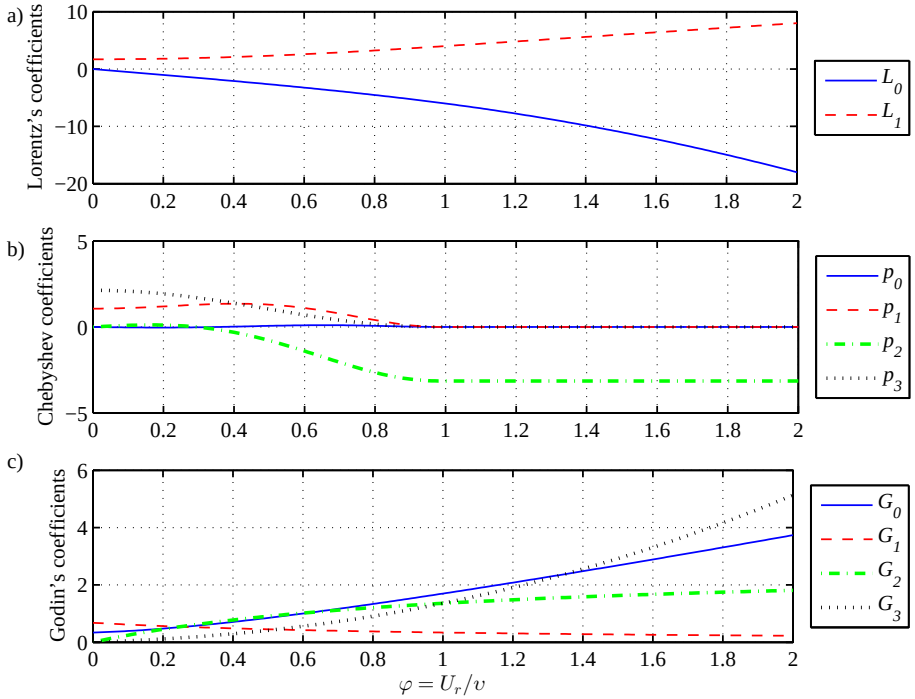

Fig. 3. Variation of the coefficients as a function of φ: **(a)** Lorentz's L_0 and L_1 (Sect. 4.2); **(b)** Chebyshev's p_0, p_1, p_2 and p_3 (Sect. 4.3); **(c)** Godin's G_0, G_1, G_2, G_3 (Sect. 4.4).

HESSD
10, 9191–9238, 2013

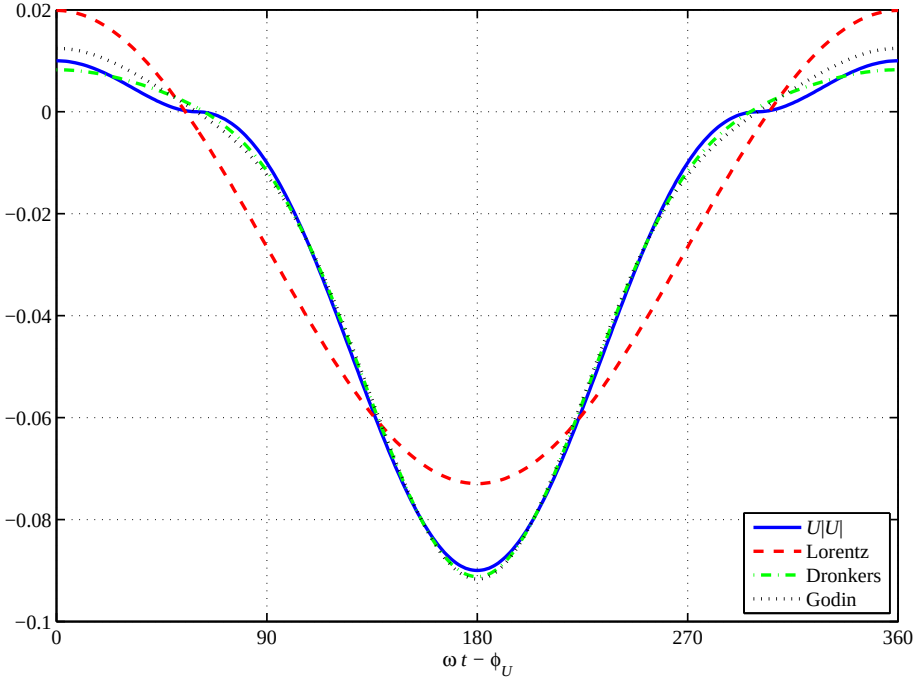

Fig. 4. Approximations of $U|U|$ by different approaches with $\varphi = 0.5$ and $\upsilon = 0.2\,\mathrm{m\,s^{-1}}$, so that $U = 0.2\cos(\omega t - \phi_U) - 0.1$.

HESSD
10, 9191–9238, 2013

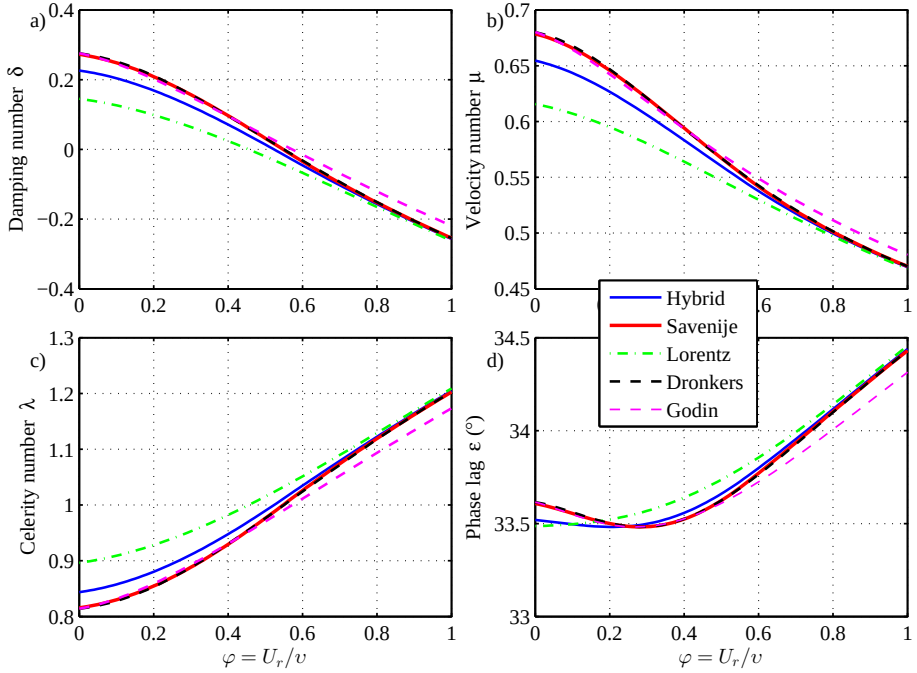

Fig. 5. The main dimensionless parameters (damping number δ, velocity number μ, celerity number λ and phase lag ε) obtained with the different analytical methods as a function of dimensionless river discharge φ with $\zeta = 0.1$, $\gamma = 1.5$, $\chi_0 = 20$ and $r_S = 1$.

HESSD
10, 9191–9238, 2013

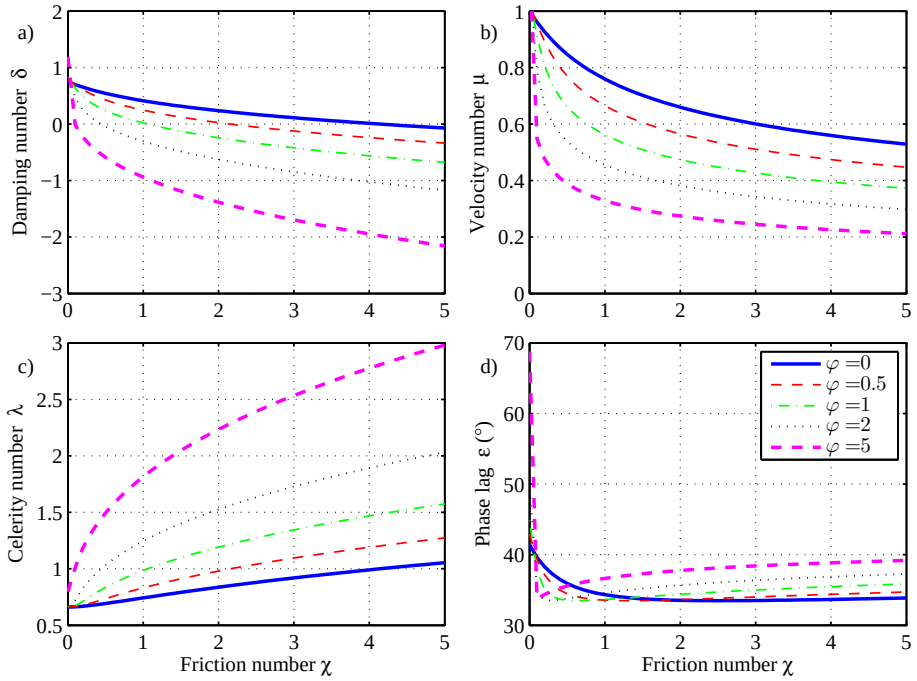

Fig. 6. Relationship between the main dimensionless parameters and the friction number χ obtained by solving the Eqs. (11) (with $\Gamma = \Gamma_H$), (37) and (38) for different values of the dimensionless river discharge term φ with $\zeta_0 = 0.1$, $\gamma = 1.5$ and $r_S = 1$.

HESSD
10, 9191–9238, 2013

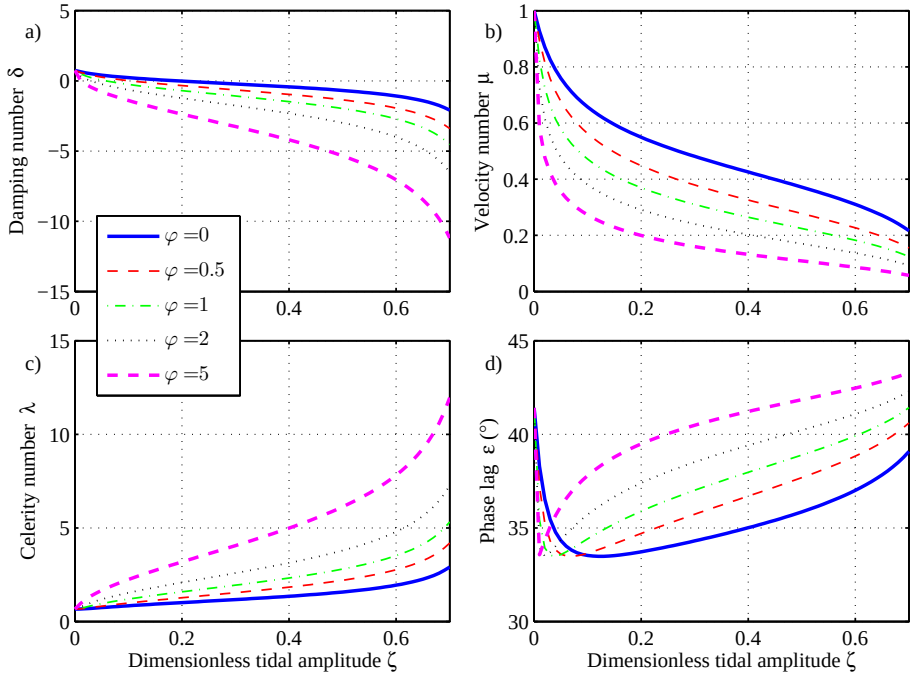

Fig. 7. Relationship between the main dimensionless parameters and the dimensionless tidal amplitude ζ obtained by solving the Eqs. (11) (with $\Gamma = \Gamma_H$), (37) and (38) for different values of the dimensionless river discharge term φ with $\chi_0 = 20$, $\gamma = 1.5$ and $r_S = 1$, where χ_0 is defined with Eq. (40).

HESSD
10, 9191–9238, 2013

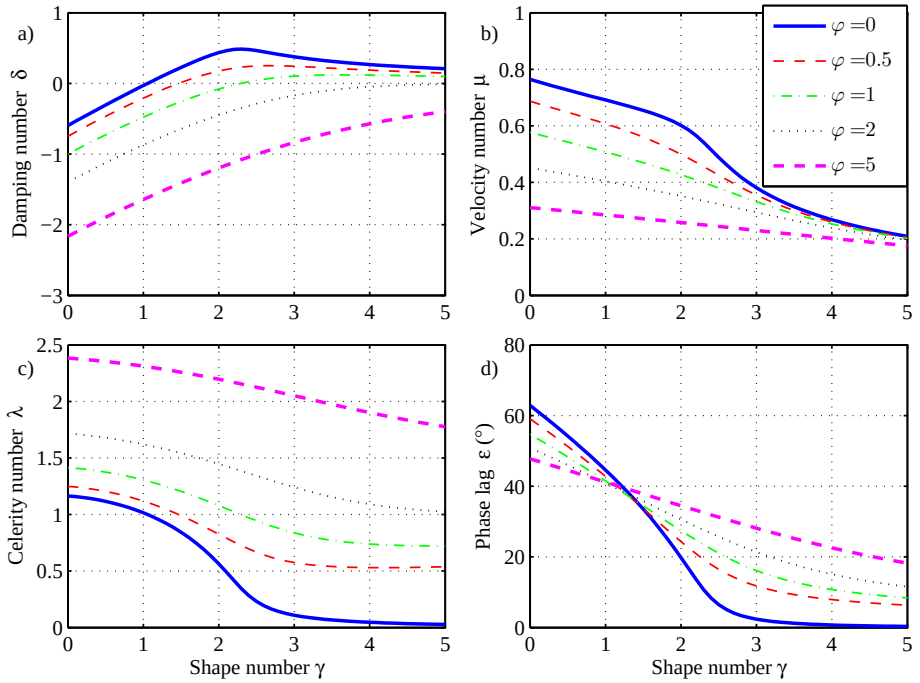

Fig. 8. Relationship between the main dimensionless parameters and the estuary shape number γ obtained by solving the Eqs. (11) (with $\Gamma = \Gamma_H$), (37) and (38) for different values of the dimensionless river discharge term φ with $\zeta_0 = 0.1$, $\chi_0 = 20$ and $r_S = 1$.

HESSD
10, 9191–9238, 2013

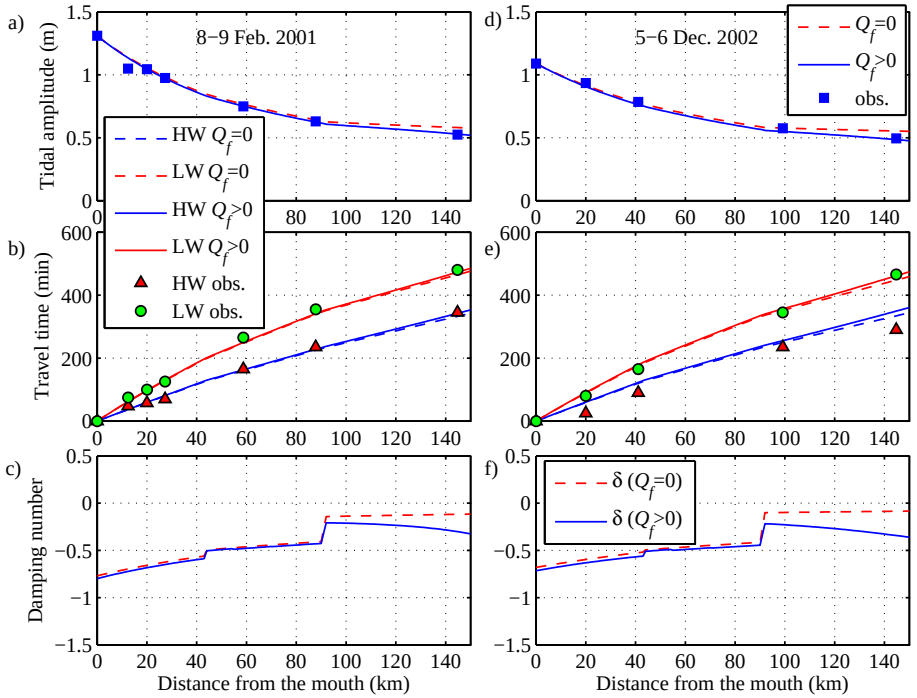

Fig. 9. Comparison of analytically calculated tidal amplitude **(a, d)**, travel time **(b, e)** with measurements and comparison of two analytical models to compute the dimensionless damping number **(c, f)** on 8–9 February 2001 (calibration) and 5–6 December 2002 (validation) in the Modaomen estuary. The dashed line represents the model where river discharge is neglected. The continuous line represents the model accounting for the effect of river discharge. Both models used the same friction coefficients calibrated while considering river discharge.

HESSD
10, 9191–9238, 2013

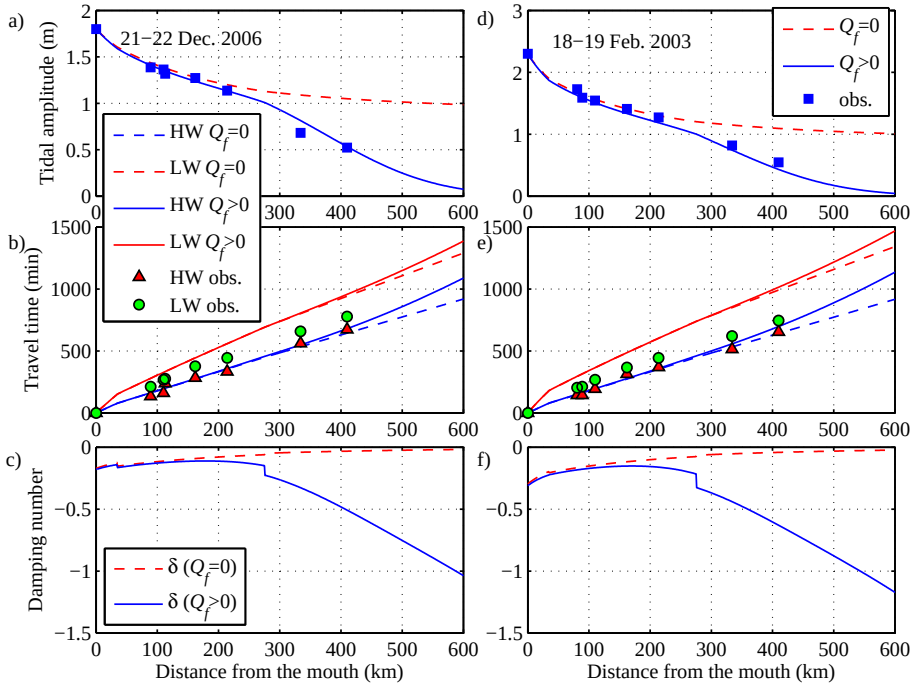

Fig. 10. Comparison of analytically calculated tidal amplitude **(a, d)**, travel time **(b, e)** with measurements and comparison of two analytical models to compute the dimensionless damping number **(c, f)** on 21–22 December 2006 (calibration) and 18–19 February 2003 (validation) in the Yangtze estuary. The dashed line represents the model where river discharge is neglected. The continuous line represents the model accounting for the effect of river discharge. Both models used the same friction coefficients calibrated while considering river discharge.

HESSD
10, 9191–9238, 2013

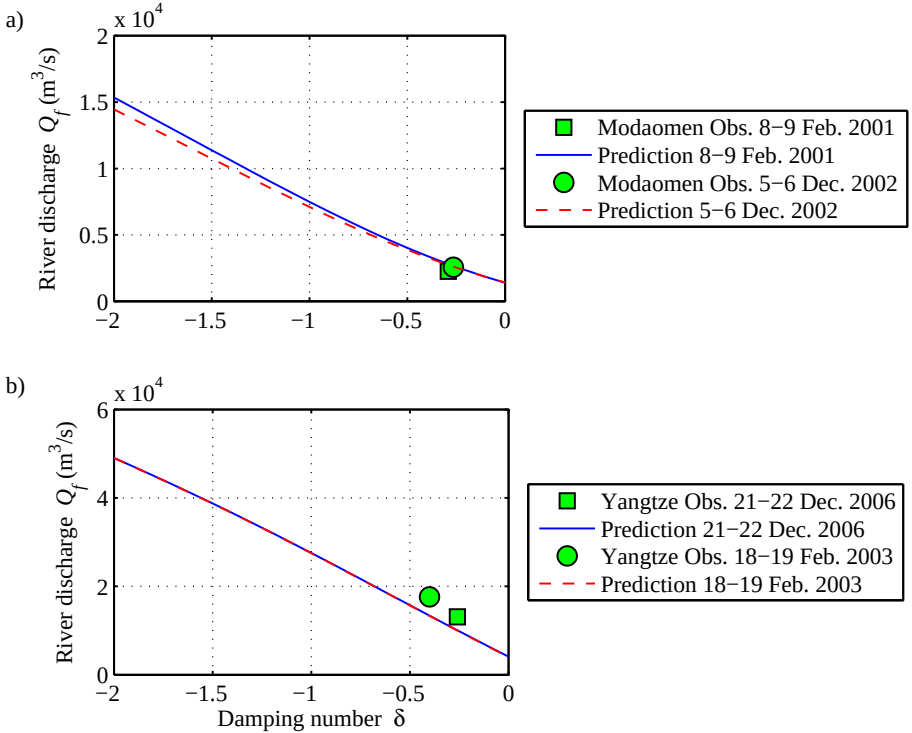

Fig. 11. Predictions of river discharge Q_f as a function of the damping number δ: **(a)** in the Modaomen estuary for given values of $K = 38\,m^{1/3}\,s^{-1}$, $\overline{h} = 10.3\,m$, $\overline{A} = 12\,000\,m^2$, $r_S = 1.3$ and $a = 110\,km$ at position $x = 116\,km$; **(b)** in the Yangtze estuary for given values of $K = 70\,m^{1/3}\,s^{-1}$, $\overline{h} = 11\,m$, $\overline{A} = 14\,100\,m^2$, $r_S = 1$ and $a = 200\,km$ at position $x = 372\,km$.

HESSD
10, 9191–9238, 2013